Dielectric Properties and 3D Printing of UV-cured Acrylic Composite with Alumina Microfiller

Muneaki Kurimoto, Hiroya Ozaki, Yuu Yamashita
Nagoya University
Department of Electrical Engineering and Computer Science
Furo-cho, Chikusa-ku, Nagoya 464-8603, Japan

Toshihisa Funabashi, Takeyoshi Kato
Nagoya University
Institute of Materials and Systems for Sustainability
Furo-cho, Chikusa-ku, Nagoya 464-8603, Japan

and **Yasuo Suzuoki**
Nagoya University
Department of Electrical Engineering and Computer Science
Furo-cho, Chikusa-ku, Nagoya 464-8603, Japan

ABSTRACT

3D printing has potential to provide various solid insulating material such as a functionally graded material. It has not been clarified if the polymer-ceramic composite, the basic structure for the solid insulating material, can be 3D-printed even when the large amount of insulating ceramics fillers are introduced. This paper investigated the feasibility of the stereolithographic 3D printing of an insulating component using a UV-cured acrylic composite with a micorometric alumina fillers (alumina/UV-cured acrylic composite). Since scattering and absorption of UV light by alumina fillers were potential obstacle to UV curing, the UV light transmission characteristics of the alumina/UV-cured acrylic composite were obtained. The result provides the evidence that UV light reaches the back side of the layer of the composite and the resin is cured. As basic dielectric properties, permittivity and loss tangent of the alumina/UV-cured acrylic composites were obtained. It was confirmed that the permittivity of the composites was in accordance with the formulas for permittivity of two-component composite. By using the composite material, a 3D model of the conical insulating spacer was designed with physics simulation software and the data was printed out.

Index Terms — **Alumina filler, UV-cured-acrylic resin, polymer composite, stereolithographic 3D printer, permittivity, UV transmission.**

1 INTRODUCTION

A Higher-performance solid insulator can be achieved not only by employing a new material but also by improving a manufacturing process. Recently, a "3D printer" attracts a renewed attention [1]. A 3D printer is a device for additive manufacturing, which is the process of joining materials to make an object from 3D model data, usually layer upon layer [2]. It has a potential to provide various solid insulators with functionally graded materials such as permittivity graded materials [3-18]. Although the industrial application of 3D printer requires further development of itself, it has a potential to realize the functionally graded materials and solid insulators whose shape and graded function cannot be formed by molding.

One of the 3D printing techniques is stereolithography in which a 3D object is printed out of thin layers of UV cured polymer. The polymer is cured layer by layer with UV-light irradiation. The polymer materials used in the stereolithography are UV-cured acrylic resin, UV-cured epoxy resin and so on. The stereolithography was proposed when the additive manufacturing was invented [19] and has been advanced technically [20]. Although there is room for the improvement of the printing material, such as weather resistance and cracking resistance, the stereolithographic 3D printer has a high accuracy and can fabricate a solid insulator without air voids inside the material. A question remains

Manuscript received on 24 November 2015, in final form 1 July 2016, accepted 1 July 2016.

whether the polymer-ceramic composite can be printed by the 3D printer even when the large amount of the ceramics fillers such as alumina and silica are introduced.

In this paper, the technical feasibility of 3D printing of an insulating component with using UV-cured-acrylic composite with micrometric alumina fillers (alumina/UV-cured-acrylic composite) was investigated. Since scattering and absorption of UV light by alumina fillers was a potential obstacle to UV curing, UV transmission characteristic of the composite was obtained. As basic dielectric properties, permittivity and loss tangent of the composite were measured. By using the alumina/UV-cured-acrylic composite in stereolithographic 3D printer, a model conical insulating spacer was fabricated to examine the feasibility of 3D printing in manufacturing functionally graded insulating components.

2 EXPERIMENTAL METHOD

2.1 FABRICATION OF ALUMINA COMPOSITE SPAMPLES

Figure 1 shows the diameter distribution of the alumina fillers used. The filler was of spherical shape with an average diameter of 15 μm. The UV-cured-acrylic matrix was based on methacrylated oligomers cured with photoinitiator. Table 1 shows the sample specifications. In the polymer composite samples, the amount of alumina fillers was changed from 0 to 40 vol%.

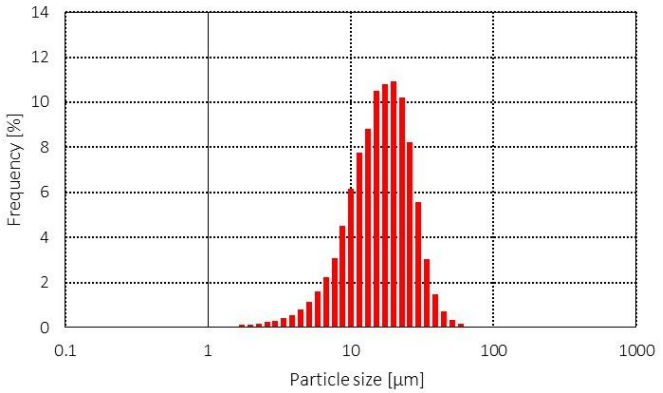

Figure 1. Diameter distribution of alumina fillers used in alumina/ UV-cured-acrylic composite.

The fabrication process of the alumina composite samples consisted of the following steps.

(1) Liquid acrylic resin was mixed with alumina fillers by a planetary mixer and degassed.

(2) The mixture was cured by the irradiation of UV light at room temperature.

(3) The specimen was postcured thermally at 70 degrees celsius.

Figure 2 shows SEM images of alumina composite samples. In the micrographs, white parts show alumina fillers and black parts show resin. It is confirmed that the SEM images show uniform dispersion of fillers and more fillers with increasing volume fraction of fillers.

Table 1. Sample specifications

Sample	Volume fraction of fillers (vs total)
Unfilled epoxy	No filler
Alumina composite 10	10 vol%
Alumina composite 20	20 vol%
Alumina composite 40	40 vol%

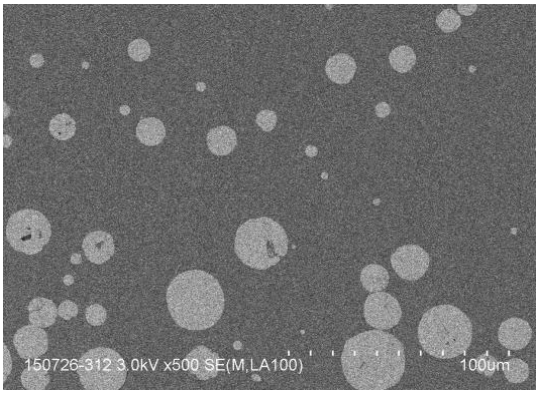

(a) Alumina composite 10

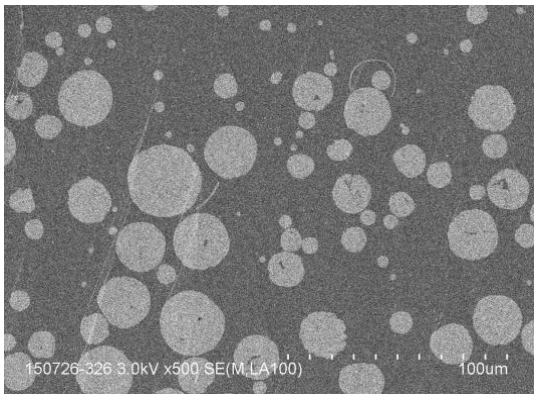

(b) Alumina composite 20

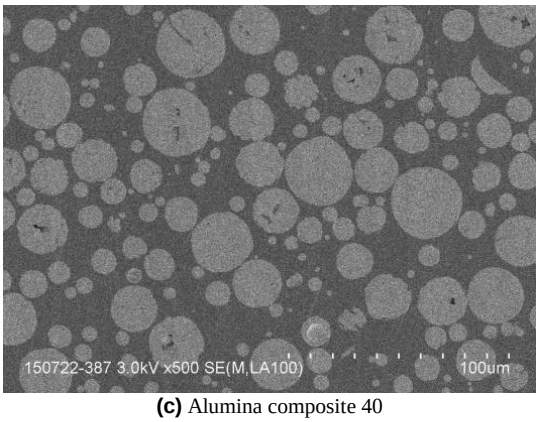

(c) Alumina composite 40

Figure 2. SEM images of alumina/ UV-cured-acrylic composite samples with different volume fraction of fillers of 10 vol% ((a) Alumina composite 10), 20 vol% ((b) Alumina composite 20), 40 vol% ((c) Alumina composite 40).

As the 3D object, we chose a conical insulating spacer which was used in the evaluation of the creeping discharge of the solid insulator [22]. The 3D model data of the conical spacer was prepared by using a finite element calculation software (COMSOL Multiphysics) and the data was printed out by the stereolithographic 3D printer.

In order to measure the UV transmittance and dielectric properties, the sheet of 0.2 mm × 50 mm × 50 mm was formed by the 3D printer. The thickness of 0.2 mm corresponds to the maximum thickness of the layer that can be formed in each step by our 3D printer.

2.2 STEREOLITHOGRAPHIC 3D PRINTER

Figure 3 shows the schematic diagram of a stereolithographic 3D printer used in the experiment. The liquid resin with alumina fillers was poured on the resin tray and was irradiated with UV light through the transparent bottom of the tray. The UV light was scanned by galvanometer mirror. The wavelength of UV light was 405 nm. While the building support plate was elevated step by step, the resin was cured layer upon layer. The thickness of the layer formed in each step was 0.1 mm.

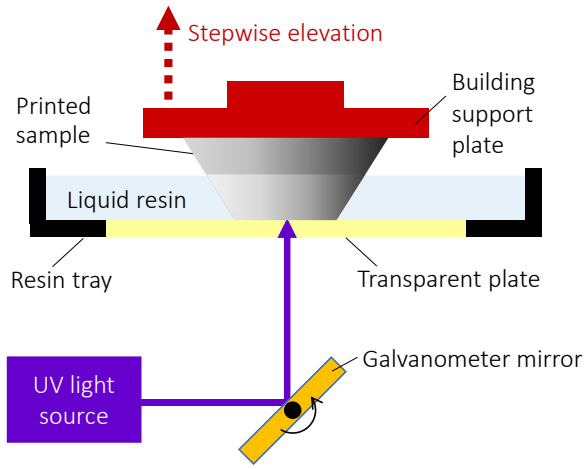

Figure 3. Schematic illustration of stereolithographic 3D printer.

.

2.3 MEASUREMENT OF UV TRANSMITTANCE AND DIELECTRIC PROPERTY

UV transmittance of the sheet samples was measured using ultraviolet-visible infrared spectrophotometer (V-570, JASCO corporation). The measurement wavelength were from 200 nm to 800 nm. Two types of transmittance was measured. One is the transmittance of the only light which goes straight through the sample (straight light). The other one is the transmittance of both the straight light and forward scattered light go through the sample. In order to detect the forward scattered light, we used the integrating sphere whose inner wall was coated with a high reflectance material. Moreover, in order to eliminate the influence of reflection by the roughness of the sheet surface, smooth polyester sheets adhere to the both sides of the sheet sample.

Dielectric permittivity was obtained from the measurement of the capacitance of the sheet samples. The aluminum electrodes with a guard ring (diameter of main electrode : 31 mm) were evaporated on both surfaces. The capacitance and dielectric loss tangent were measured from 100 Hz to 1 MHz under the measuring voltage of 1.5 V.

3 EXPERIMENTAL RESULTS AND DISCUSSIONS

3.1 UV TRANSMISSION CHARACTERISTICS

Figure 4 shows the light transmission characteristics of unfilled resin sample. The transmittance of both the straight

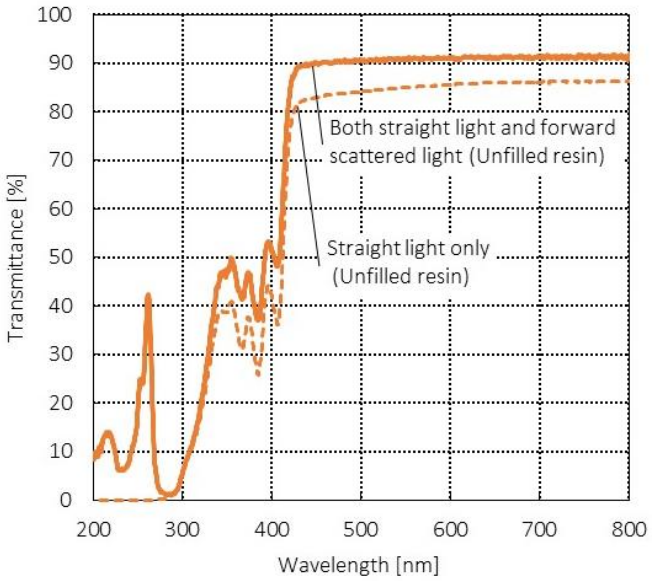

Figure 4. Transmittance of straight light and forward scattered light through the sheet sample of unfilled resin.

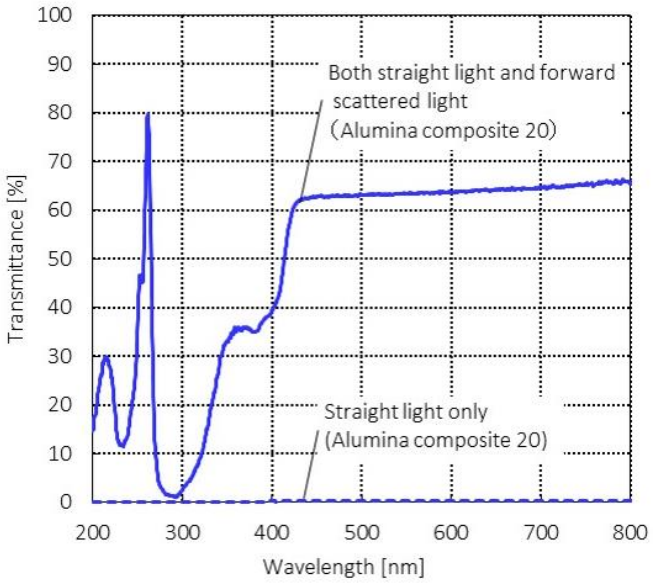

Figure 5. Transmittance of straight light and forward scattered light through the sheet sample of alumina composite 20.

light and the forward scattered light was slightly higher than that of the straight light only. The transmittance of both the straight light and forward scattered light in the 400 nm-500 nm range was 48-91 %.

Figure 5 shows the light transmission characteristics of alumina composite 20. The transmittance of the straight light was less than 0.5 %. It is considered to be due to the scattering and absorption of UV light by alumina fillers. However, the transmittance of both the straight light and the forward scattered light was higher than that of the straight light. In particular, the transmittance of both the straight light and the forward scattered light in the 400-500 nm range was 39-63 %. Therefore, the forward scattering of UV light by the alumina filler with the average diameter of 15 μm inside the resin is dominant. This scattering can be explained by the Mie scattering. The UV light reaches the back side of the 0.2 mm thickness sheet sample which is thicker than the layer step of 0.1 mm in the 3D printer we used. The acrylic resin is cured by UV light even when the alumina fillers are added to the resin.

Figure 6 shows the light transmission characteristics of the alumina composite samples with different volume fractions of fillers. The light transmission characteristics include the straight light and the forward scattered light and are ranged from 300 to 500 nm. With the increase of the volume fraction of fillers, the transmittance decreases. However, even when the volume fraction of fillers is 40 vol%, the transmittance of alumina composite is 35 % at 405 nm which is the wavelength used in the 3D printer. This provides the evidence that UV light reaches the back side of the layer of the composite resin and the resin is cured.

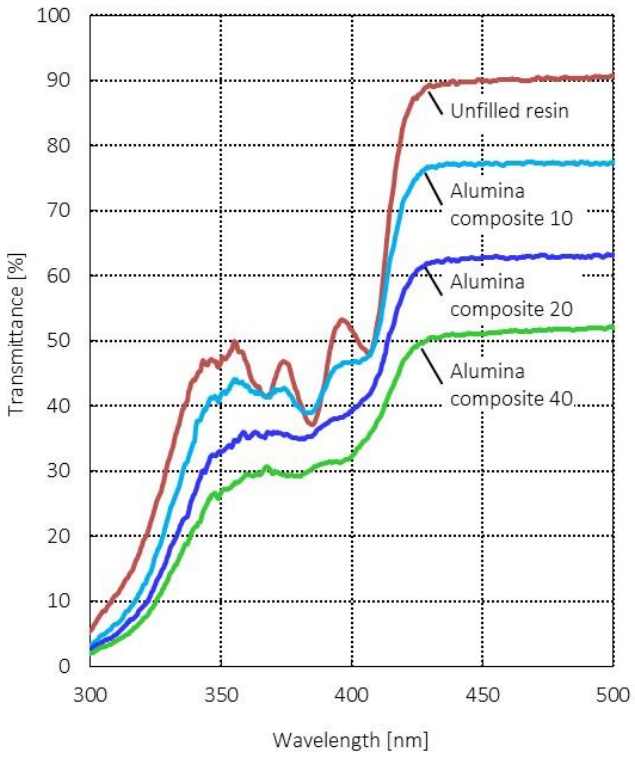

Figure 6. Transmittance of straight light and forward scattered light through the sheet sample of unfilled resin and the alumina composite with different volume fractions of fillers.

3.2 DIELECTRIC PERMITTIVITY AND DIELECTRIC LOSS TANGENT

Figure 7 shows the frequency dependence of the relative permittivity of the unfilled resin and the alumina composites. The permittivity of the alumina composite is higher than that of the unfilled resin. In particular, the permittivity at 1 MHz of alumina composite (40%) is 5.6, which is higher than that of unfilled epoxy, 3.8. This is explained by the higher permittivity of alumina (10) than the unfilled resin. Figure 8 shows the frequency dependence of the dielectric loss tangent. Dielectric loss tangent of the alumina composite is lower than that of the unfilled resin. This is because alumina filler has lower dielectric loss tangent (0.0002) than unfilled resin [23].

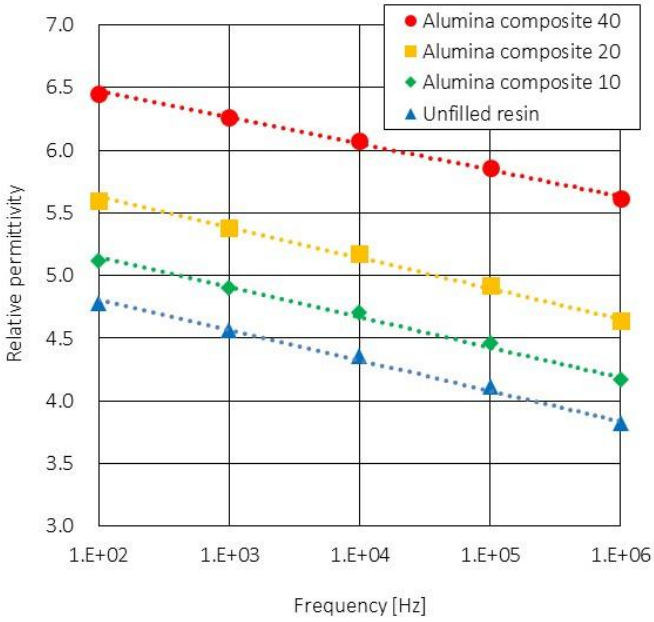

Figure 7. Frequency dependence of relative permittivity of unfilled resin and the alumina composite with different volume fraction of filler.

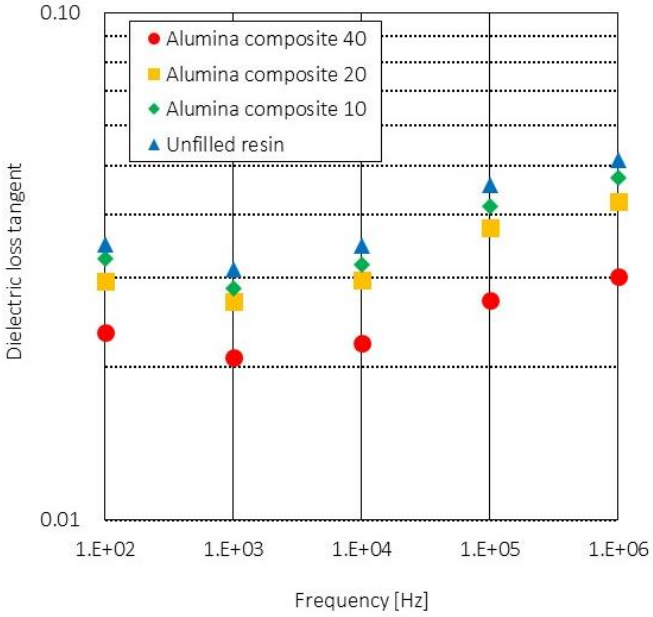

Figure 8. Frequency dependence of dielectric loss tangent of unfilled resin and the alumina composites with different volume fractions of fillers.

Figure 9 shows the dependence of relative permittivity at 1 MHz on the volume fraction of alumina. In order to verify the experimental data was reasonable, we compared the experimental data with the models of permittivity of two-media composite, such as parallel capacitor model, series capacitor model, random arranged model, Lichitenecker-Rother equation and Bruggeman equation [24, 25]. The permittivity of the parallel capacitor model is calculated by assuming that the two components are expressed by two capacitors in parallel virtually, corresponds to the maximum of the permittivity of two media composite. The permittivity of the series capacitor model corresponds to the minimum. Similarly, the series capacitor model assumed two capacitors in series. The permittivity of the random arranged model is a geometric average of the parallel capacitor model and the series capacitor model. The random arranged model, Lichitenecker-Rother equation and Bruggeman equation are used for estimation of permittivity of polymer composite. Figure 10 shows the permittivity increases with the increase of the volume fraction of alumina fillers. The experimental data are between the parallel capacitor model and the series capacitor model and are in accordance with the random arranged model, Lichitenecker-Rother equation and Bruggeman equation.

Figure 10 shows the volume fraction dependence of dielectric loss tangent at 1 MHz of the unfilled resin and the alumina composite. The dielectric loss tangent decreases with the increase of the volume fraction of alumina fillers. The experimental data are compared with the parallel capacitor model, the series capacitor and random arranged model. In the calculation models, dielectric loss tangent of alumina material was assumed to be 0.0002. The experimental data of the alumina composite is between the parallel capacitor model and the series capacitor model and is close to the random arranged model.

3.3 STEREOLITHOGRAPHIC 3D PRINTING OF CONICAL INSULATING SPACER MODEL

A conical insulating spacer model was designed to have the height of 10 mm, the lower base diameter of 40 mm and the contact angle of 45 degree. This model is often used to evaluate the surface insulation characteristics such as flashover voltage. Figure 11 shows the FEM model. The triangles on the spacer surface are finite element meshes for electric field analysis. Figure 12 shows the electric field around conical insulating spacer calculated by FEM. The relative permittivity of the spacer is 4.2 which is the same as that of sheet sample of alumina composite 10. Electric field enhancement was confirmed around triple junction (TJ) of electrode, gas and spacer. The FEM model was printed out by the stereolithographic 3D printer.

Figure 13 shows the conical insulating spacer printed out by the stereolithographic 3D printer. Although the asperity on the spacer surface due to the layer-by-layer printing was observed, the contact angle at TJ was 45 ± 0.5° which was accurate enough to evaluate the surface insulation characteristics, e.g. flashover voltage.

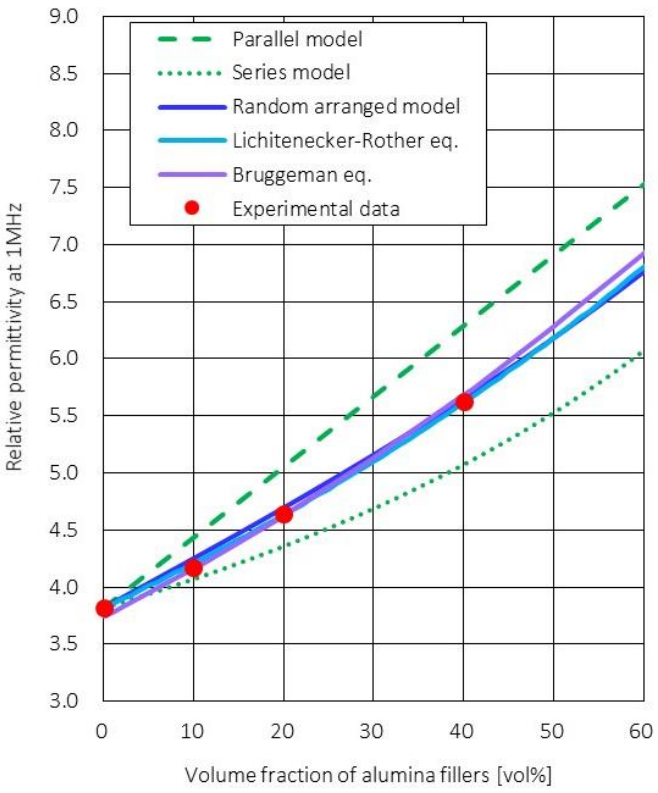

Figure 9. Relative permittivity at 1 MHz as function of volume fraction of filler volume in alumina composite.

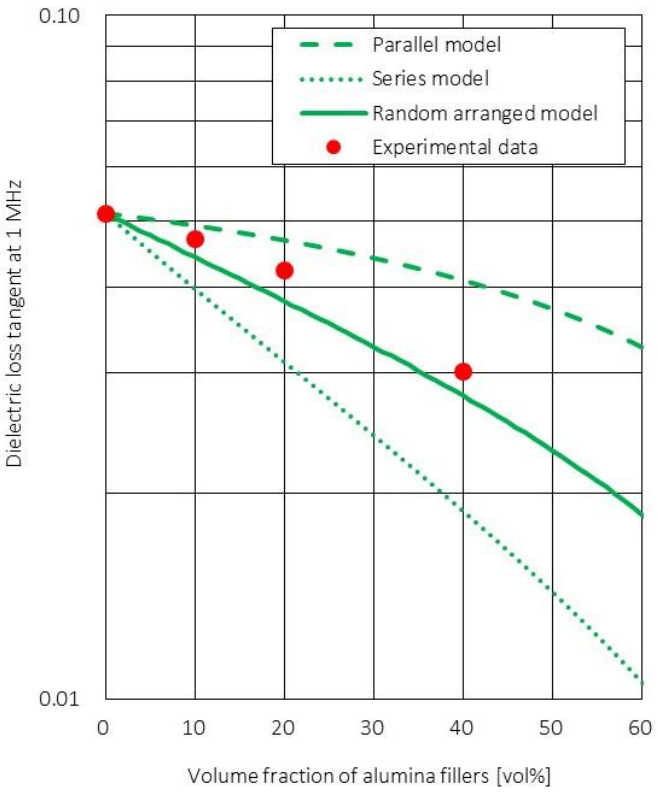

Figure 10. Dielectric loss tangent at 1 MHz as function of volume fraction of fillers in alumina composite.

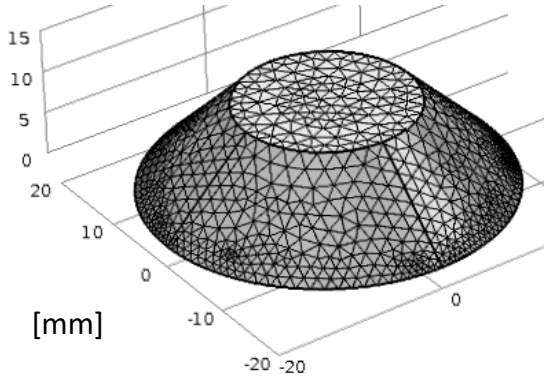

Figure 11. FEM model of conical insulating spacer.

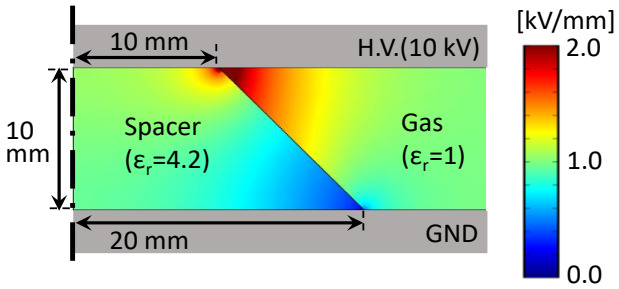

Figure 12. Electric field around conical insulating spacer. (Material: alumina composite 10).

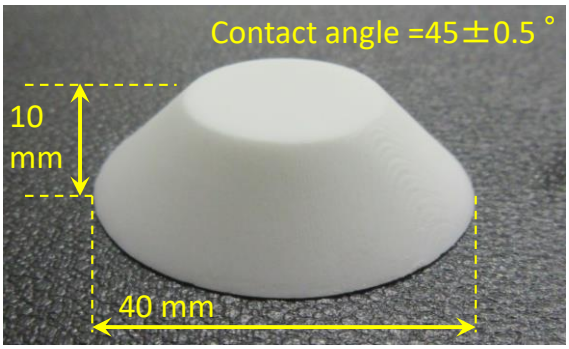

Figure 13. Conical insulating spacer by stereolithographic 3D printing (alumina composite 10).

In order to confirm the volume fraction of alumina fillers inside the printed spacer, the specific gravity of the conical spacer was measured. Figure 14 shows the specific gravity of the conical spacers made of unfilled resin and alumina composite. The specific gravity of the spacer increased with increasing the volume fraction of alumina in the mixture used for the 3D printing, indicating the introduction of alumina fillers to the spacer.

From the specific gravity of the spacers, the volume fraction of alumina fillers inside the spacer is calculated as equation (1).

$$\frac{V_f}{100} = \frac{\rho_c - \rho_r}{\rho_{al} - \rho_r} \qquad \cdots (1)$$

V_f is volume fraction of alumina fillers [vol%], ρ_r is specific gravity of acrylic resin (g/ml), ρ_c is specific gravity of the

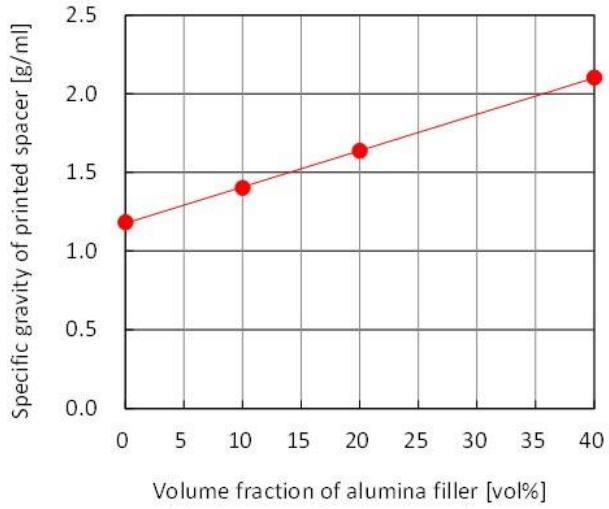

Figure 14. Specific gravity of the conical spacer of unfilled resin and alumina composite.

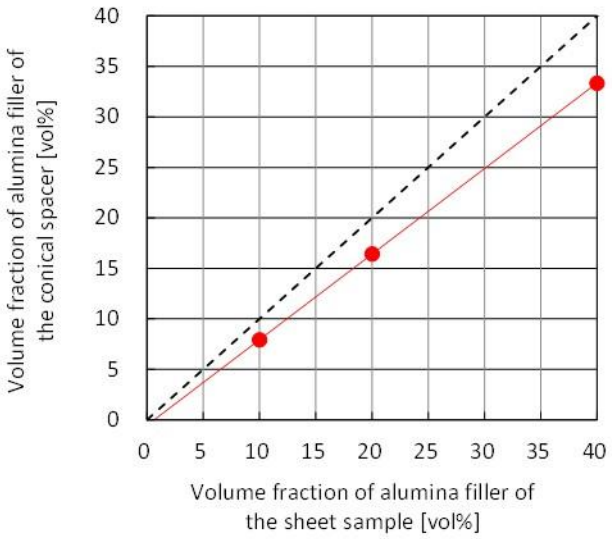

Figure 15. Difference of volume fraction of alumina fillers between the conical spacer and the sheet sample..

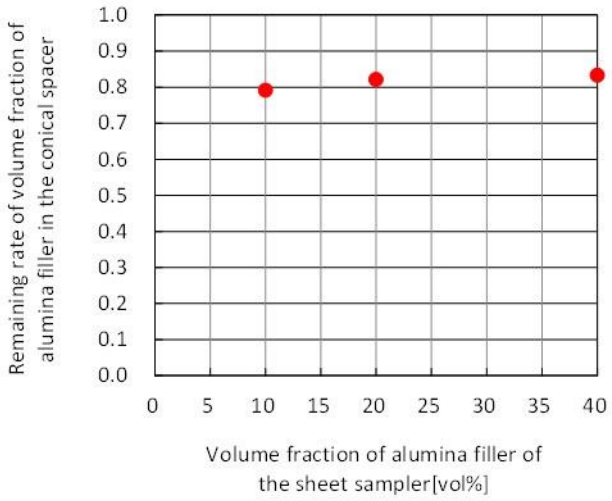

Figure 16. Remaining rate of volume fraction of alumina fillers of the conical insulating spacer.

composite specimen (g/ml), ρ_{al} is specific gravity of alumina material (3.95 g/ml). Figure 15 shows the measured value of V_f inside the spacer sample as a function of V_f inside the sheet samples made with the same mixing ratio of resin and fillers. V_f of the spacer sample is less than that of the sheet sample.

The remaining rate of V_f in the spacer sample is obtained by dividing V_f inside the spacer sample by V_f inside the sheet sample. Figure 16 shows the remaining rate is about 0.8. It is consider that the part of alumina fillers (with the diameter of several tens of μm) sediments and are not taken in the cured layer during the printing process. From this results, it is confirmed that the particle diameter is important for the 3D printing of the composite. This can be improved by optimizing the particle diameter distribution or shortening the printing time [20].

4 CONCLUSIONS

The technical feasibility of the stereolithographic 3D printing of an insulating component was investigated by using UV-cured-acrylic composite with micorometric alumina filler. By using the sheet samples of alumina/UV-cured-acrylic composite, UV transmission characteristics and dielectric properties were evaluated. The conical insulating spacer model, which was often used to evaluate the surface insulation characteristics such as flashover voltage, made of the alumina composite were printed out by the stereolithographic 3D printer. The main results are summarized as follows.

(1) The UV transmission characteristics revealed that UV light was transmitted through the composite system even when the amount of alumina fillers with average diameter of 15 μm was 40 vol%. This demonstrates the feasibility of using a stereolithographic 3D printer to manufacture alumina composites by UV curing.

(2) It was confirmed that the permittivity of the alumina composite increased with the increase of filler volume fraction. The tendency is in accordance with the formula of permittivity of two component composite. This indicates the possibility that the flexible control of permittivity distribution in functional graded material can be achieved by 3D printing.

(3) Although the particle diameter distribution need to be optimized, it was demonstrated that the stereolithographic 3D printer could produce a prototype of the conical insulating spacer with height of 10 mm using the alumina composite with micrometric alumina fillers with average diameter of 15 μm.

ACKNOWLEDGMENT

This research work was partly supported by a research grant from the Naito Science & Engineering Foundation.

REFERENCES

[1] C. Anderson, *Makers: The New Industrial Revolution*, Crown Business, 2012.

[2] ASTM F2792-12a, “Standard Terminology for Additive Manufacturing”.

[3] K. Kato, K. Kimura, S. Sakuma and H. Okubo, "Functionally Gradient Material (FGM) For GIS Spacer Insulation", 12th Int’l. Sympos. High Voltage Eng., Vol.2, pp.401-404, 2001.

[4] K. Kato, M. Kurimoto, K. Kimura, S. Sakuma and H. Okubo, "Experimental Study on Permittivity Graded Spacer for Control of Electric Field Distribution", 12th Int’l. Sympos. High Voltage Eng., Vol. 2, pp. 549-553, 2001.

[5] K. Kato, M. Kurimoto, H. Adachi, S. Sakuma and H. Okubo, "Impulse Breakdown Characteristics of Permittivity Graded Solid Spacer in SF6", IEEE Conf. Electr. Insul. Dielectr. Phenomena, pp. 401-404, 2001.

[6] M. Kurimoto, K. Kato, H. Adachi, S. Sakuma and H. Okubo, "Fabrication and Experimental Verification of Permittivity Graded Solid Spacer for GIS", IEEE Conf. Electr. Insul. Dielectr. Phenomena, pp.789-792, 2002.

[7] H. Okubo, M. Kurimoto, H. Shumiya, K. Kato, H. Adachi and S. Sakuma, "Permittivity Gradient Characteristics of GIS Solid Spacer", 7th Intnl. Conf. on Properties and Applications of Dielectr. Materials, Paper S1-3, 2003.

[8] H. Shumiya, K. Kato and H. Okubo, "Feasibility Study on FGM Application for Gas Insulated Equipment", IEEE Conf. Electr. Insul. Dielectr. Phenomena, Paper 5A-6, 2004.

[9] H. Shumiya, K. Kato, H. Okubo, "Fabrication and Prediction tehiniques for FGM Application to Solid Insulators", IEEE Conf. Electr. Insul. Dielectr. Phenomena, Paper 7C-1, 2005.

[10] H. Okubo, H. Shumiya, M. Ito and K. Kato, "Insulation Performance of Permittivity Graded FGM in SF6 Gas under Lightning Impulse Conditions", IEEE Int’l. Sympos. Electr. Insul., pp.332-335, 2006.

[11] H. Okubo, H. Shumiya, M. Ito and K. Kato: "Optimization Techniques on Permittivity Distribution in Permittivity Graded Solid Insulators", IEEE Int’l. Sympos. Electr. Insul., pp. 519-522, 2006.

[12] K. Kato, M. Kurimoto, H. Shumiya, H. Adachi, S. Sakuma and H. Okubo, “Application of Functionally Graded Material for Solid Insulator in Gaseous Insulation System”, IEEE Trans. Dielectr. Electr. Insul. , Vol.13, No. 1, pp. 362-372, 2006.

[13] M. Kurimoto, A. Kai, K. Kato and H. Okubo, “Fablication of Permittivity Graded Materials for Reducing Electric Stress on Electrode Surface”, IEEE Int’l. Sympos. Electr. Insul., pp. 265-268, 2008.

[14] H. Okubo, K. Kato, N. Hayakawa, M. Hanai and M. Takei, “Functionally Graded Materials and their Applications to High Electric Field Power Equipment”, CIGRE SC D1 – Colloquium, Hungary Budapest, D1-101, 2009.

[15] M. Kurimoto, K. Kato, M. Hanai, Y. Hoshina, M. Takei and H. Okubo, “Application of Functionally Graded Material for Reducing Electric Field on Electrode and Spacer Interface”, IEEE Trans. Dielectr. Electr. Insul., Vol.17, No.1, pp. 256-263, 2010.

[16] H. Hama, S. Okabe, M. Miyashita and H. Okubo, “Aging evaluation of insulation materials for environmentally-friendly compact gas-insulated equipment”, CIGRE Paris Session, D1-110, 2012.

[17] N. Hayakawa, K. Kato, H. Okubo, H. Hama, Y. Hoshina and T. Rokunohe, “Electric Field Grading Techniques in Power Apparatus Using Functional Materials”, CIGRE Paris Session, D1-309 (2014)

[18] J. Ishiguro, M. Kurimoto, H. Kojima, K. Kato, H. Okubo and N. Hayakawa, “Electric Field Control in Coaxial Disk-Type Solid Insulator by Functionally Graded Materials”, IEEE Conf. Electr. Insul. Dielectr. Phenomena, pp. 663–666, 2014.

[19] H. Kodama, “Automatic method for fabricating a three-dimensional plastic model with photo-hardening polymer”, Rev. Scientific Instrum., Vol. 52, No. 11, pp.1770-1773, 1981.

[20] J. R. Tumbleston, D. Shirvanyants, N. Ermoshkin, R. Janusziewicz, A. R. Johnson, D. Kelly, K. Chen, R. Pinschmidt, J. P. Rolland, A.Ermoshkin, E. T. Samulski and J. M. DeSimone, “Continuous liquid interface production of 3D objects”, Science, Vol. 347, No. 6228, pp.1349-1351, 2015.

[21] M. Kurimoto, Y. Yamashita, H. Ozaki, T. Kato, T. Funabashi and Y. Suzuoki, “3D Printing of Conical Insulating Spacer with Using Alumina/Polymer Composite”, Annual meeting of the Institute of Electr. Eng., Japan, Vol. 2, No. 2-015, pp.19, 2015 (in Japanese).

[22] K. Kato, M. Kurimoto, K. Kimura, S. Sakuma and H. Okubo, “Experimental Study on Permittivity Graded Spacer for Control of Electric Field Distribution”, 12th Int’l. Sympos. High Voltage Eng., Vol. 2, pp. 549-553, 2001.

[23] R. C. Weast, *Handbook of Chemistry and Physics*, CRC press, pp.E-60, 1980.

[24] G. G. Raju, *Dielectrics in Electric Fields*, Marcel dekker, inc., pp.80-81, 2003.

[25] M. Kurimoto, T. Kawashima, H. Suzuki, Y. Murakami and M. Nagao, "Dielectric Permittivity Characteristic of Mesoporous-Alumina/Epoxy Composite", IEEE Conf. Electr. Insul. Dielectr. Phenomena, pp. 307-310, 2012.

Muneaki Kurimoto (M'10) was born in 1978. He received the B.Sc. degree in 2001, the M.S. degree in 2003 and the Doctor of Eng. degree in 2010, all in electrical engineering, from Nagoya University, Japan. From 2003 to 2007, he joined Aisin Seiki Corporation, Japan. From 2010 to 2013, he was an Assistant Professor at Toyohashi University of Technology, Japan. Since 2013, he has been an Assistant Professor at Nagoya University. He is a member of IEE of Japan and IEEE.

Hiroya Ozaki was born in 1992. He received the B.Sc. degree in electrical engineering in 2014 from Nagoya University, Nagoya, Japan. Since 2014, he is a M.S. degree student in electrical engineering at Nagoya University. He is a student member of IEE of Japan.

Yuu Yamashita (S'14) was born in 1991. He received the B.Sc. degree in electrical engineering in 2014 from Nagoya University, Nagoya, Japan. Since 2013, he is a M.S. degree student in electrical engineering at Nagoya University. He is a student member of IEE of Japan and IEEE.
.

Takeyoshi Kato (M'09) was born in 1968. He received the B.Sc. degree in 1991, the M.S. degree in 1993 and the Doctor of Eng. degree in 1996, all in electrical engineering, from Nagoya University, Japan. From 1996 to 2015, he was on the faculty of Nagoya University, Japan. Since 2015, he has been a Professor at Nagoya University. He is a member of IEE of Japan and IEEE.

Toshihisa Funabashi (M'90-SM'96) was born in Aichi, Japan in 1951. He received the B.S. degree from Nagoya University, Japan, in 1975, and the Ph.D. degree from Doshisha University, Kyoto, Japan, in 2000, both in electrical engineering. From 1975 to 2014, he joined Power System Engineering Division, Meidensha Corporation, Tokyo, Japan. Since 2014, he has been a Professor at Nagoya University. He is a member of IEE of Japan, IET and IEEE.

Yasuo Suzuoki (M'94) was born in 1950. He received the B.S. degree in 1973, the M.S. degree in 1975 and the Doctor of Eng. degree in 1978, all in electrical engineering, from Nagoya University, Nagoya, Japan. From 1978 to 1995, he was on the faculty of Nagoya University. From 1995 to 2016, he was a Professor at Nagoya University. At present, he is a Professor at Aichi Institute of Technology. He is a member of IEE of Japan and IEEE.